Published on 09 September 2014. Downloaded by National Physical Laboratory (NPL) on 24/04/2015 06:57:42.

PCCP

ROYAL SOCIETY OF CHEMISTRY

PAPER

View Article Online
View Journal | View Issue

Cite this: *Phys. Chem. Chem. Phys.*, 2014, **16**, 21804

Effect of low thermal budget annealing on surface passivation of silicon by ALD based aluminum oxide films

Vandana,* Neha Batra, Jhuma Gope, Rajbir Singh, Jagannath Panigrahi, Sanjay Tyagi,† P. Pathi, S. K. Srivastava, C. M. S. Rauthan and P. K. Singh*

Received 1st August 2014,
Accepted 18th August 2014

DOI: 10.1039/c4cp03430a

www.rsc.org/pccp

Thermal ALD deposited Al_2O_3 films on silicon show a marked difference in surface passivation quality as a function of annealing time (using a rapid thermal process). An effective and quality passivation is realized in short anneal duration (~100 s) in nitrogen ambient which is reflected in the low surface recombination velocity (SRV <10 cm s^{-1}). The deduced values are close to the best reported SRV obtained by the high thermal budget process (with annealing time between 10–30 min), conventionally used for improved surface passivation. Both as-deposited and low thermal budget annealed films show the presence of positive fixed charges and this is never been reported in the literature before. The role of field and chemical passivation is investigated in terms of fixed charge and interface defect densities. Further, the importance of the annealing step sequence in the MIS structure fabrication protocol is also investigated from the view point of its effect on the nature of fixed charges.

1. Introduction

In a semiconductor, recombination losses occur largely *via* defect levels within the band gap. These defects are located in the bulk material and at the surfaces (largely due to the presence of dangling bonds). The reduction of such losses is of prime importance for numerous photonic devices such as light emitting diodes, photo-detectors and photovoltaic cells.[1] The losses emanating from the two surfaces can be reduced by surface passivation and is an area to be addressed for making efficient next generation devices. In order to reduce the cost of silicon solar cells made on expensive wafers (high quality silicon), thinner substrates (to reduce the usage in terms of watt g^{-1}) are required.[2,3] A reduction in thickness and surface modification (either by anisotropic[4] or nano-texturisation[5]) to reduce reflection losses leads to the increase of the surface to volume ratio and, consequently, the surface recombination becomes a dominant loss factor.[6] This affects the solar cell performance parameters adversely. Recently, surface passivation is becoming increasingly important to enhance the performance of both single crystal (c-Si) and multi-crystalline silicon (mc-Si) solar cells.[2] Passivation reduces surface recombination losses by two ways, *i.e.*, chemical passivation (reduction of the density of electronic surface states) and field effect passivation (the presence of fixed charges in the dielectric layer over the silicon surface that reduces the carrier density underneath the interface of the two).[1,7–10] A well passivated surface reduces the recombination of photo-generated carriers in the vicinity of the two surfaces and improves the cell performance parameters.[11–14] Thermally grown silicon oxide (SiO_2), silicon nitride (a-SiN_x:H) and amorphous silicon (a-Si:H) are commonly used for surface passivation of c-Si solar cells.[15–21] Aluminum oxide (Al_2O_3), a dielectric, has excellent surface passivation properties on c-Si of both conductivity type materials.[7–9] Recently Al_2O_3 films have been used to passivate the silicon surface to achieve high efficiency solar cells.[11–14] There are several methods for Al_2O_3 film deposition, *e.g.*, sputtering,[22] atmospheric pressure chemical vapor deposition,[23] RF magnetron sputtering[24] and plasma enhanced chemical vapour deposition,[25,26] *etc.* Atomic layer deposition (ALD) has been proven to be a valuable technique for the growth of Al_2O_3 thin films.[27] ALD is a conformal coating technique, by which a high level of control over film thickness and uniformity can be achieved besides being a low temperature process. There are several reports related to the surface passivation property of Al_2O_3 films deposited using thermal ALD process.[1,7–9] The measure of surface passivation is surface recombination velocity (SRV) which can be deduced from the measured minority carrier lifetime values. Although in some papers, low SRV is obtained in as-deposited Al_2O_3 films,[28] however, high quality surface passivation is realized after post deposition annealing.[1,7–9] Normally 30 min post-deposition

Silicon Solar Cell Group, (Network of Institutes for Solar Energy), CSIR - National Physical Laboratory, New Delhi-110012, India. E-mail: vandana1@nplindia.org, pksingh@nplindia.org
† The author is working at Central Electronics Limited, Sahibabad, India.

 This journal is © the Owner Societies 2014

Published on 09 September 2014. Downloaded by National Physical Laboratory (NPL) on 24/04/2015 06:57:42.

annealing at 400 °C is required to get good surface passivation. To the best of our knowledge, low thermal budget annealing is very scantly reported in the literature. Further, the reported studies in the past are different in terms of deposition parameters and conditions, therefore, show different performances in as-deposited and annealed states. All this indicates that the passivation mechanism is not yet fully understood and is not straightforward for as-deposited and annealed films. The overall performance is explained either individually or as a combined effect of chemical and field effect passivation which are described in terms of interface defect and fixed charge densities respectively.[1,7–9]

In this paper, the study of c-Si surface passivation by Al_2O_3 film is reported. The Al_2O_3 films of different thickness are deposited to optimize post-annealing time (t_{anl}) at a fixed annealing temperature (T_{anl} = 400 °C). The effect of the film thickness on effective minority carrier lifetime and refractive index is investigated. The minority carrier lifetime is measured from which SRV values (at Al_2O_3/Si interface) are deduced which defines effectiveness of surface passivation. *C–V* measurements are used to find the flat band voltage (V_{FB}), density of fixed charges (Q_F) and interface defects (D_{it}).

2. Experimental

To grow Al_2O_3 thin films, trimethylaluminum [TMA, $(Al(CH_3)_3)$] (procured from M/s SAFC, Hitech, UK) and H_2O (deionised water of 18.3 MΩ cm) are the precursors used for aluminum and oxygen sources respectively. The films are deposited in a thermal ALD reactor (Model: R200, M/s Picosun, Finland). The films are grown on float zone (FZ) n- and p-Si (325 ± 10 μm thick) substrates of (100) orientation and resistivity (5 ± 0.5 Ω cm). In order to ensure exactly the same optical and electronic properties, each sample is a quarter diced from chemically mechanically polished (CMP) 100 mm diameter wafer. The samples are cleaned with piranha solution (PC, $H_2SO_4 : H_2O_2$::4 : 1 solution for 15 min) followed by 2 min dip in diluted HF (5% solution). A single deposition cycle in the ALD system consists of two half cycles; one TMA pulse and the other H_2O pulse and each half cycle is separated by a nitrogen purge step. During each cycle, one monolayer of the material is formed and as the number of cycle progresses, the number of mono-layers grows one over another. After deposition of the desired thickness of the layer on one side, the sample is flipped after taking it out from the deposition chamber to load lock, in order to get the film deposited on the rear side also. The film of the same thickness is grown on the rear side. Samples (S_1–S_5) of various thicknesses are prepared by varying the number of deposition cycles (details are given in Table 1). The substrate temperature (T_{sub}) is fixed at 300 °C during the deposition. Post-deposition annealing (T_{anl}) is carried out at 400 °C (commonly used and optimized during the course of study) in nitrogen ambient by rapid thermal processing (RTP Model: AS-one 150, M/s Annealsys, France).

The film thickness ($d_{Al_2O_3}$) and refractive index ($n_{Al_2O_3}$) are measured by a spectroscopic ellipsometer (Model: M2000, M/s J.A. Wollam Co. Inc., USA). The reflectivity of the films is measured using a spectrophotometer fixed with an integrating sphere (Model: PVE 300, M/s Benthem, UK with an integrating sphere DTR6). To ensure the correctness of the measured reflectivity values, the measurements are done after baseline (*i.e.*, back ground) correction using standard high purity $BaSO_4$ powder pressed in the form of a pallet. Fourier transform infrared spectroscopy (Model 2000, M/s Perkin Elmer spectrometer, USA) is used to get information about the surface bonding.

Table 1 The number of precursor cycles and corresponding film thickness ($d_{Al_2O_3}$) and refractive index ($n_{Al_2O_3}$) of films made on n-Si

Sample	No. of cycles	Thickness (nm)	Refractive index
S_1	1000	93.1	1.65
S_2	500	48.0	1.64
S_3	300	30.1	1.62
S_4	100	11.2	1.53
S_5	50	7.2	1.50

The minority carrier lifetime (τ_{eff}) is measured using the photo-conductance decay method (Model: WCT-120, Sinton lifetime tester) and the uniformity of τ_{eff} is examined by mapping the lifetime parameter using a microwave photoconductive decay system (μW-PCD, Model: WT 2000, M/s Semilab Zrt, Hungary). τ_{eff} measured by Sinton's lifetime tester is an effective average value of carrier lifetime. In this tool, excess carriers are generated by a flash and the sheet conductivity is measured by RF coil inductively coupled to the sample. The flash intensity and sheet conductivity are converted into a generation rate of electron–hole (e–h) pairs and the average excess carrier density by using the mobility model.[29] In the WCT-120 injection levels (Δn) can be varied in a wide range ($10^{13} < \Delta n < 10^{16}$ cm^{-3}). The system operates in (i) quasi steady state photo-conductance (QSSC) and (ii) transient photo-conductance (TPC) decay modes. In the QSSC mode, the decay constant of the flash should be at least 10 times slower than the carrier lifetime so that the population of excess carriers attains a steady state and hence, the lifetime is measured under steady state conditions. In the transient mode, the fast pulse of light which peaks and decays back in ~15 μs is used and the photo-conductance decay is measured to determine the effective carrier lifetime. This mode is suitable for high lifetime materials. Transient mode is used when the measured lifetime values are more than 200 μs and the quasi steady state mode is used in the low lifetime values.[30] To see the lifetime uniformity, measurements are also made using μW-PCD which has a 904 nm pulsed laser (penetration depth >30 μm) and a microwave source operating at 10 GHz are used. The former is for optical excitation and the later for signal detection (where decay of the excess carrier concentration is monitored by the microwave reflectance). In this system the injection level is fixed (Δn = 1.2 × 10^{13} cm^{-3}). Hence, the measured τ_{eff} by the WCT-120 and the μW-PCD could be compared at the same injection levels.[31]

The metal–insulator–semiconductor (MIS) structure (schematic of which is given in Fig. 1) is fabricated by depositing aluminum dots (area ~0.02 cm^2) using an e-beam evaporation system

Published on 09 September 2014. Downloaded by National Physical Laboratory (NPL) on 24/04/2015 06:57:42.

Fig. 1 Schematic of the MIS structure. Different thicknesses of Al_2O_3 layers are used.

(M/s Hind Hivac, India). The capacitance–voltage (C–V) measurements are performed with an impedance/gain phase analyzer (Model: 1260, M/s Solartron, UK).

3. Results and discussion

3.1. Film thickness and the refractive index

The atomic force (AFM) and scanning electron (SEM) microscopes studies reveal that the ALD deposited films are highly conformal and uniform. A typical atomic force micrograph of S_3 is given in Fig. 2. The RMS surface roughness is ∼5 Å which is almost the same as that of the substrate (chemically mechanically polished silicon wafer) within measurement uncertainty.

The measured film thickness and refractive index as a function of number of deposition cycles are shown in Fig. 3. A linear growth (@0.09 nm per cycle) of film thickness as a function of the number of process cycles is observed which is indicative of highly controlled film growth. The refractive index also changes with the number of cycles and increases with increase in the film thickness. Refractive index values are rather low at lower film thicknesses and stabilizes for $d_{Al_2O_3}$ ∼ 30 nm. The ellipsometric measurements at times are sensitive to a perturbation parameter at low thicknesses.[32] In the reported values, this aspect is taken care by the error bars. The measured $d_{Al_2O_3}$ and $n_{Al_2O_3}$ values are effective values rather than the true estimation of the parameters (as described below).

Although Al_2O_3 is thermodynamically stable on silicon, however, growth of a SiO_2 or an aluminum silicate layer at the Al_2O_3/Si interface is inevitable as the growth occurs under non-equilibrium conditions.[27] It is observed that initially the thickness of the interfacial layer increases and stabilizes at 1–2 nm[7,27] during Al_2O_3 film growth. The interfacial layer affects the refractive index and the measured $n_{Al_2O_3}$ may be that of the Al_2O_3–SiO_2 composite layer. The low refractive index for thinner Al_2O_3 ALD film thicknesses is attributed to this interfacial layer. Once the thickness of the interfacial layer stabilizes, the value of n is close to the refractive index of bulk alumina (∼1.77) within measurement error and the measured value is close to the values reported in ALD deposited Al_2O_3 films.[27] The annealing of the films does not change either the thickness or the refractive index. This further reiterates the conformity and compactness of the thermally grown films. The typical monolayer thickness of Al_2O_3 is 0.3 nm and the growth rate 0.09 nm per cycle is quite low, albeit similar growth rates are given in the literature.[27]

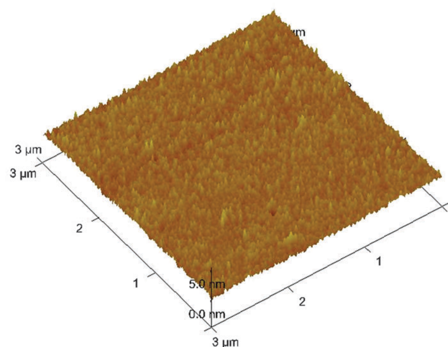

Fig. 2 AFM micrograph of S_3 with 30 nm thick Al_2O_3 layer on CMP wafer.

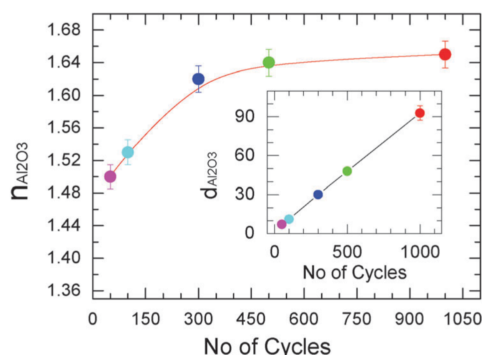

Fig. 3 Refractive index as a function of the number of ALD cycles. The inset shows film thickness (in nm) with number of cycles.

3.2. Reflectivity

Fig. 4 shows spectral dependence of the reflectivity (R_λ) of samples S_1–S_4 along with that of reference CMP silicon wafer. It is observed that surface reflectivity does not change much at a lower Al_2O_3 thickness (<10 nm) and is close to the value of the CMP sample, but the increase in $d_{Al_2O_3}$ reduces R_λ. An overall reduction in R_λ is observed in a 400 to 1050 nm range. However, minima of R_λ shifts from ∼400 nm to ∼600 nm with change in the film thickness from ∼30 nm to ∼93 nm. The average reflectance reduces from 32.8% (CMP-Si) to 32.13%, 27.98%, 21.4%, and 16.8% respectively for samples S_4, S_3, S_2 and S_1. The minimum R_λ is ∼4% for sample S_1. This trend is expected in single layer coating.

The position (wavelength, λ_{min}) of the minimum in R_λ is related to the thickness and the refractive index by the

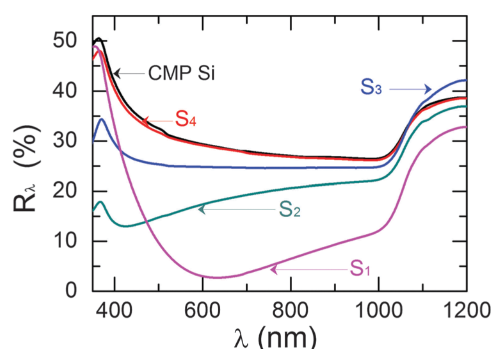

Fig. 4 Reflectivity of samples S_1–S_4 along with that of a CMP wafer.

This journal is © the Owner Societies 2014

relationship; $\lambda_{\min} = 4d_{Al_2O_3} \times n_{Al_2O_3}$.[33,34] On the other hand, in the regions away from $\lambda_{\min}$, a combined effect of constructive (*i.e.*, $2d_{Al_2O_3} \times n_{Al_2O_3}/\lambda = 2\pi$) and destructive (*i.e.*, $2d_{Al_2O_3} \times n_{Al_2O_3}/\lambda = \pi$) interferences prevails depending on the path length (extent of $d_{Al_2O_3}$ and $n_{Al_2O_3}$ values) that decides the magnitude of R_λ.[33–35] For example, the value of $\lambda_{\min}$ is estimated using the measured $d_{Al_2O_3}$ (=93 nm) and $n_{Al_2O_3}$ (=1.65) and is found to be 614 nm for sample S_1. This value is the same (=630 ± 2.5% nm) as determined in S_1 by spectroscopic measurements within measurement uncertainty. The shift in the $\lambda_{\min}$ position is the manifestation of the change in $d_{Al_2O_3}$ and $n_{Al_2O_3}$. It can be noted that there is a systematic change in R_λ with the increase in the thickness of the film particularly in the 450 to 1000 nm range.

Although ALD is generally adopted to deposit ultra thin films, reflectivity studies are carried out to observe the effect of film thickness and their potential to work as an antireflection coating (ARC) in conjunction with passivation properties.

3.3. FTIR spectroscopy

Fig. 5 shows the transmittance FTIR spectra of samples S_1–S_4. The broad absorption band in the range of 600–400 cm^{-1} is attributed to the Al–O stretching in the characteristic spectra of Al_2O_3. It is reported that a band at 564 cm^{-1} results from two unresolved structures at 562 and 565 cm^{-1}. The first one is assigned to Al–O bending for AlO_6 (5 + 1), while the second to a pure Al–O stretching mode for AlO_4.[36] The peak observed in the 560–570 cm^{-1} region (a minor shift with $d_{Al_2O_3}$) represents Al–O modes. On the other hand, the observed peak in 670–700 cm^{-1} may be attributed to Al–O stretching mode.[37,38] The absorption peak at ~710 cm^{-1} corresponds to the Al–O stretching mode.[37,38] The peak at 1040–1060 cm^{-1} is attributed to Si–O–Si.[37] An absorbance peak due to Al=O at ~1345 cm^{-1} (as shown in the inset of the figure) is also present[39] but is rather weak whereas in some other reports this peak is not detected.[37] In all the samples, FTIR spectra show characteristic peaks of Al_2O_3.

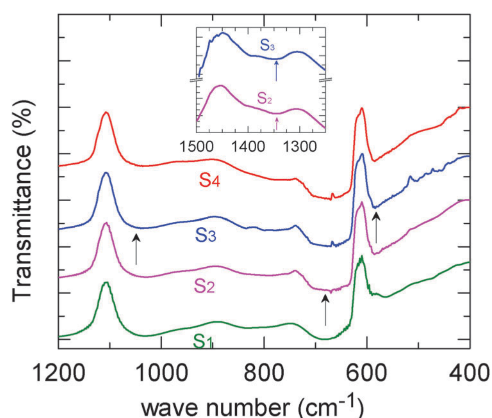

Fig. 5 FTIR spectra of samples S_1–S_4. The inset shows an absorbance peak at ~1345 cm^{-1} due to Al=O.

3.4. Minority carrier lifetime

The measured minority carrier lifetime value has contributions from the bulk (τ_b) and the surface recombination lifetime (τ_s) associated with the wafer surfaces which are related to each other by the following relation;[31,40]

$$\frac{1}{\tau_{\text{eff}}} = \frac{1}{\tau_b} + \frac{1}{\tau_s}$$

where τ_s is equal to $(D_p\beta^2)^{-1}$, which in turn is related to surface recombination velocity S through the relation $\beta\tan(\beta d/2) = S/D_p$. Here D_p is the diffusion coefficient. In the case of high lifetime material, measured τ_{eff} is predominantly a measure of surface recombination.

To evaluate the surface passivation, the upper limit of S_{eff} is determined from the effective lifetime at an injection level (Δn) equal to 10^{15} cm^{-3} by assuming bulk lifetime very large. Therefore, S_{eff} gives the worst estimate of the SRV value. Fig. 6 gives a typical photo-conductive decay curve used for the determination of effective lifetime by Sinton's lifetime tester in the transient mode.

It is known that annealing conditions play an important role in surface passivation performance. To optimize the film annealing conditions, a rapid thermal processing technique (RTP) is used which is a low thermal budget process. For a given set of

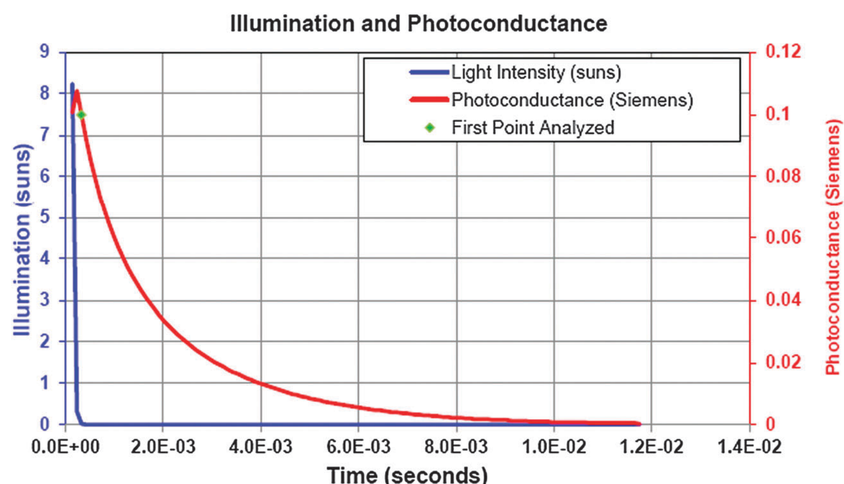

Fig. 6 A typical photo-conductive decay curve obtained by Sinton's lifetime tester in transient mode.

Published on 09 September 2014. Downloaded by National Physical Laboratory (NPL) on 24/04/2015 06:57:42.

experiments, annealing temperature is fixed at 400 °C and annealing time (t_{anl}) is varied.

Fig. 7(a–c) show effective minority carrier lifetime (τ_{eff}) data as a function of the injection level for as-deposited and annealed samples S_2, S_3 and S_4 respectively for different annealing time (t_{anl}) at fixed T_{anl} = 400 °C. Lifetime data show a good quality passivation in the entire injection level range (5×10^{13} to 1×10^{16} cm^{-3}) in all the three samples. The value of τ_{eff} in un-passivated samples is 18 and 1.5 μs for n- and p-Si respectively which is controlled by SRV values (that is high SRV $> 10^3$ cm s^{-1} in Table 2, and $> 10^4$ cm s^{-1} in ref. 41). An interesting observation is that the measured τ_{eff} value increases for shorter sintering time duration, attains its maximum (in the vicinity of 100 s) and on further increase in t_{anl}, the value of τ_{eff} starts decreasing. This trend is observed in all the samples. Therefore, optimized sintering time for the best passivation is 105 s. It is to be noted that in most of the publications,[1,7–10,27] annealing is done for longer time durations (10–30 min) and there is hardly any publication for shorter t_{anl}.

Published on 09 September 2014. Downloaded by National Physical Laboratory (NPL) on 24/04/2015 06:57:42.

Table 2 Measured minority carrier lifetime (τ_{eff}) and the upper limit of surface recombination velocity (SRV) values for as-deposited samples, at injection level, $\Delta n = 1 \times 10^{15}$ cm^{-3}. The values of τ_{eff} and SRV have ~4% error in their estimation

	n-Si		p-Si	
Sample	τ_{eff} (μs)	SRV (cm s^{-1})	τ_{eff} (μs)	SRV (cm s^{-1})
Bare	18	903	1.5	10 833
S_1	2244	7	820	20
S_2	1102	15	678	24
S_3	824	20	430	38
S_4	471	35	337	48
S_5	103	158	149	109

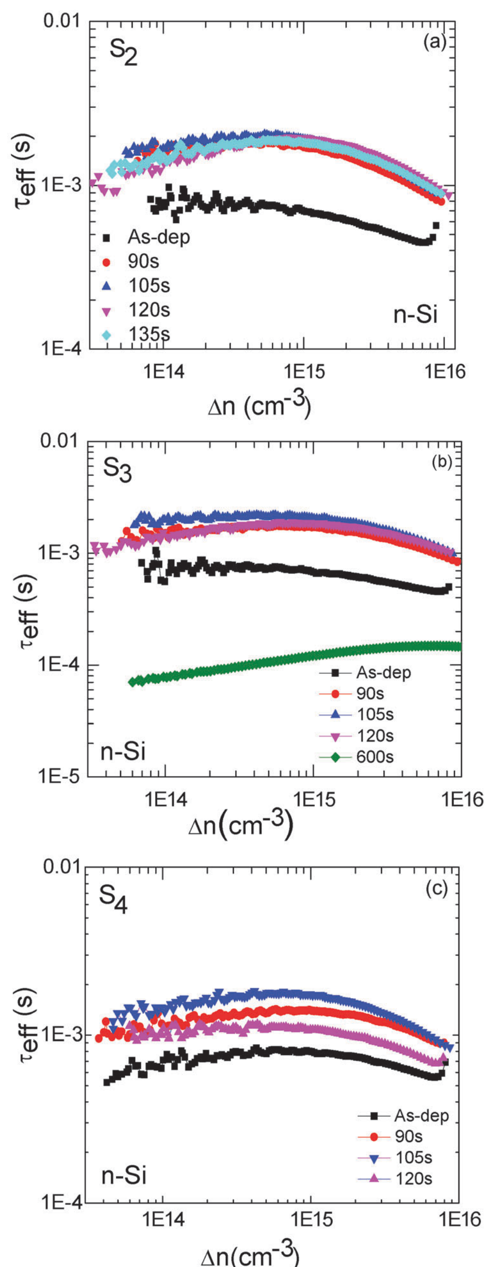

Fig. 7 The measured minority carrier lifetime (τ_{eff}) as a function of the injection level (Δn) for n-Si samples, t_{dep} = 300 °C and T_{anl} = 400 °C, The data for S_2 (a) as-deposited and 90, 105, 120 and 135 s annealed, for S_3 (b) as-deposited and 90, 105, 120 and 600 s annealed and for S_4 (c) as-deposited and 90, 105 and 120 s annealed.

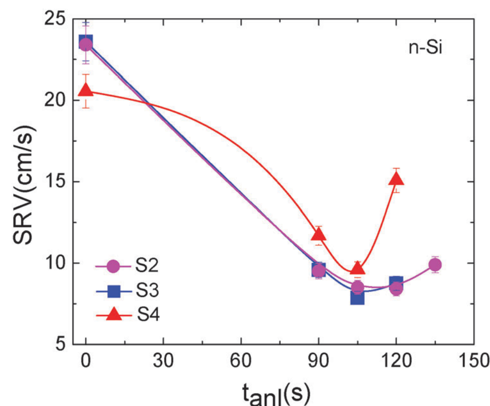

Fig. 8 SRV as a function of sintering time (t_{anl}) for sample S_2, S_3 and S_4. T_{anl} = 400 °C.

Table 2 summarizes the measured minority carrier lifetime and corresponding estimated SRV values with films of different thicknesses. It is observed that increase in film thickness improves the surface passivation and a good surface passivation is realized in as-deposited thick films. For example, the lowest SRV values (<10 cm s^{-1}) are obtained in sample S_1 (Table 1, n-Si). A similar trend is observed in both n- and p-Si. Surface recombination velocity values for S_2, S_3 and S_4 samples with annealing duration shows minimum at ~105 s and the SRV increases both at lower and higher t_{anl} as can be seen from Fig. 8. Fig. 9 gives an idea about the uniformity of τ_{eff} over the sample area where mapping of τ_{eff} by the μ-PCD is shown for sample S_3.

3.5. Capacitance–voltage measurements: effect of the annealing sequence

Capacitance measurement as a function of voltage (C–V) is important because it gives vital information about the passivation at the

 This journal is © the Owner Societies 2014

Published on 09 September 2014. Downloaded by National Physical Laboratory (NPL) on 24/04/2015 06:57:42.

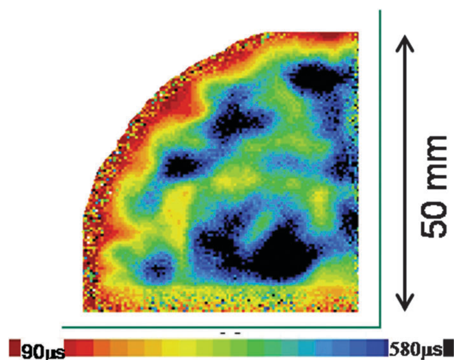

Fig. 9 μ-PCD lifetime map of sample S_3. Figure shows passivation uniformity across the wafer.

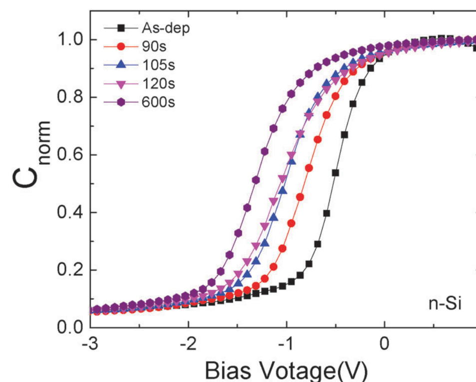

Fig. 11 Normalized *C–V* curves for S_3 measured at 1 MHz for as-deposited and annealed films at 90 s, 105 s, 120 s and 600 s using S_{AF} protocol.

Al_2O_3/Si interface.[1,7–10] The MIS structure is used for *C–V* measurements where there is an important step of metal contact formation. Two different experiments (*i.e.*, post and pre-annealing prior to metal contact formation) are carried out to see the effect of the annealing step on *C–V* characteristics. The MIS structure is made by creating a polka dot pattern of Al over the Al_2O_3 film as described under "Experimental". In the first experiment the annealing step (10 min in N_2 ambient) is done after depositing Al metal whereas in the second experiment the Al_2O_3 film is annealed (10 min in N_2 ambient) prior to the formation of metal contacts. The former is referred to as S_{MF} and the later as S_{AF} in the subsequent text. Fig. 10 shows the *C–V* data for an as-deposited sample and the two annealed samples; S_{MF} and S_{AF}.

There is a decrease in oxide capacitance in the S_{MF} sample in contrast to the increase in oxide capacitance with S_{AF} condition. Another important observation is that the flat band voltage position is opposite in the two cases. In the sample, where annealing is done prior to metal deposition (S_{AF}) shows positive charge activation. Contrary to this, activation of negative charges occurs when contacts are made prior to annealing (S_{MF}). When aluminum contact is made on the Al_2O_3 films and subsequent annealing (S_{MF}) is performed, Al metal may diffuse into the aluminum oxide film that may cause decrease in the capacitance. On the other hand, since the Al_2O_3 film is annealed prior to the formation of metal contacts (S_{AF}), no high temperature step is involved after metal deposition. In this case the possibility of Al diffusion into Al_2O_3 is completely ruled out. Consequently, higher capacitance is measured and the *C–V* data provide a better idea about the film quality and interface properties. Therefore, in the *C–V* study, the protocol of S_{AF} is followed.

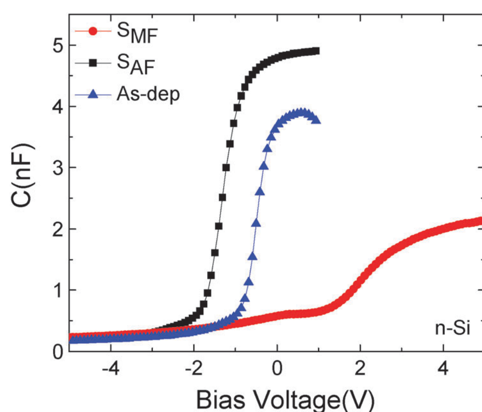

Fig. 10 Capacitance–voltage curves for S_3. The values are measured in as-deposited and in the two annealed samples; S_{MF} and S_{AF} at 1 MHz.

As mentioned earlier that silicon surface passivation using Al_2O_3 films owes to the combined effect of the field and chemical passivation, which is described in terms of fixed charge density and interface defect density respectively. Field effect passivation is provided by fixed charges located near the Si/Al_2O_3 interface whereas chemical passivation is attributed to hydrogenation at the interface, film relaxation, Si–O bond rearrangement or additional oxide growth which may work individually or in tandem.[27] Fig. 11 shows normalized *C–V* curves of MIS structures made on as-deposited and annealed Al_2O_3 films (t_{anl} = 90, 105, 120 and 600 s) on S_3 ($d_{Al_2O_3} \sim 30$ nm).

The *C–V* measurements are carried out at 1 MHz frequency. A negative shift (on abscissa) in the *C–V* curve with annealing confirms activation of positive fixed charges in the Al_2O_3 film on InGaAs substrate.[42] Low thermal annealing is not very well explored besides observance of post-annealing activation of positive (+ve) charges. Only few publications reported activation of positive charges. Further, the film capacitance increases with annealing as compared to the as-deposited sample. Table 3 compiles the parameters extracted from *C–V* measurement data. Fixed charge density calculated using the flat band shift shows an increase (in Q_F) from 0.36×10^{12} cm^{-2} to 1.34×10^{12} cm^{-2} whereas interface defect

Table 3 Fixed charge density (Q_F) and interface defect density (D_{it}) in as-deposited & sintered sample S_3, T_{sint} = 400 °C, n-Si substrate

T_{anl} (s)	Q_F ($\times 10^{12}$) cm^{-2}	D_{it} ($\times 10^{12}$) states/eV cm^2
0	0.36	2.96
90	0.91	1.8
105	1.22	1.4
120	1.34	1.5
180	0.93	2.3
300	0.96	3.5
600	1.59	3.3

Published on 09 September 2014. Downloaded by National Physical Laboratory (NPL) on 24/04/2015 06:57:42.

density, D_{it}, decreases from 2.96 × 10^{12} eV^{-1} cm^{-2} to 1.5 × 10^{12} eV^{-1} cm^{-2} with t_{anl} variation from 0 to 120 s. It is reasonable to assume that both chemical and field effects co-exist in Al_2O_3 surface passivation. A change in D_{it} and Q_F values with t_{anl} gives indication that the two effects work in tandem. An increase in Q_F with t_{anl} is observed till 120 s followed by marginal decrease thereafter. An opposite trend is observed in D_{it} values. The best results (maximum τ_{eff} and the lowest SRV) could be obtained in the range where Q_F is maximum and D_{it} is minimum. In the present case, maximum and minimum values of Q_F and D_{it} are equal to 1.34 × 10^{12} cm^{-2} and 1.4 × 10^{12} eV^{-1} cm^{-2} respectively corresponding to t_{anl} 120 s and 105 s respectively. Therefore, the best τ_{eff} or SRV could be realized at t_{anl} between 105 and 120 s. But for larger annealing duration (>180 s), the Q_F is practically the same and D_{it} increases which results in an effective decrease in τ_{eff}. For 600 s annealing, although Q_F is higher which is rather surprising as compared to the value obtained after 120 s annealing, D_{it} also becomes large (twice compared to the value corresponding to 120 s). The two acts in opposite directions and therefore the net effect is degradation in passivation performance (as could be seen in Fig. 7(b)). The magnitude of Q_F gets altered after annealing in either direction. On the other hand, D_{it} is expected to rise if the passivating species (attached to silicon surface or at the interface) get detached with the increase in annealing time. Therefore, the quality of surface passivation is a trade-off between the field effect and chemical passivation and the best passivation (maximum τ_{eff} or minimum SRV) could be realized when Q_F and D_{it}, the two quantifying parameters, attain their respective maximum and minimum values at the same annealing temperature. Further, the presence of positive charges may be attributed to the existence of Al interstitials and O vacancies. This is in good agreement with the ionic nature of the Al_2O_3.[1,10]

4. Conclusions

Silicon surface passivation is studied using Al_2O_3 thin films of various thicknesses deposited on the silicon substrate at 300 °C. The τ_{eff} values show improvement in surface passivation which is also reflected in SRV values and reflectivity measurements show its utility as an antireflection coating. *C–V* measurement data show the importance of the annealing step sequence in determining true information about the deposited films. The optimization of process parameters of the Al_2O_3 film reveals that ∼105 s annealing time gives best passivation results at 400 °C wherein Q_F = 1.22 × 10^{12} cm^{-2} and D_{it} = 1.4 × 10^{12} eV^{-1} cm^{-2}. Therefore, the best surface passivation (maximum τ_{eff} or minimum SRV) could be obtained for annealing time in the vicinity of 100 s and indeed is a trade-off between the field effect (high Q_F) and chemical passivation (low D_{it}). The low thermal budget process (like rapid thermal anneal) activates positive fixed charges (as confirmed by *C–V* data measurements). The presence of positive charges supports the existence of Al interstitials and O vacancies as the primary mechanism for surface passivation of crystalline silicon.

Acknowledgements

This work was carried out under the NWP-55 grant from Council of Scientific and Industrial Research, India under TAPSUN initiative. NB also thanks CSIR for the research fellowship.

References

1 B. Hoex, J. J. H. Gielis, M. C. M. van de Sanden and W. M. M. Kessels, *J. Appl. Phys.*, 2008, **104**, 113703.
2 A. G. Aberle, *Prog. Photovoltaics*, 2000, **8**, 473–487.
3 International Technology Roadmap for Photovoltaic (ITRPV) 2014; http://www.itrpv.net.
4 P. K. Singh, R. Kumar, M. Lal, S. N. Singh and B. K. Das, *Sol. Energy Mater. Sol. Cells*, 2001, **71**, 103–113.
5 S. K. Srivastava, D. Kumar, Vandana, M. Sharma, R. Kumar and P. K. Singh, *Sol. Energy Mater. Sol. Cells*, 2012, **100**, 33–38.
6 B. Hoex, A. J. M. van Erven, R. C. M. Bosch, W. T. M. Stals, M. D. Bijker, P. J. van den Oever, W. M. M. Kessels and M. C. M. van de Sanden, *Prog. Photovoltaics*, 2005, **13**, 705–712.
7 B. Hoex, S. B. S. Heil, E. Langereis, M. C. M. van de Sanden and W. M. M. Kessels, *Appl. Phys. Lett.*, 2006, **89**, 042112.
8 G. Agostinelli, A. Delabie, P. Vitanov, Z. Alexieva, H. F. W. Dekkers, S. DeWolf and G. Beaucarne, *Sol. Energy Mater. Sol. Cells*, 2006, **90**, 3438–3443.
9 B. Hoex, J. Schmidt, P. Pohl, M. C. M. van de Sanden and W. M. M. Kessels, *J. Appl. Phys.*, 2008, **104**, 044903.
10 K. Matsunaga, T. Tanaka, T. Yamamoto and Y. Ikuhara, *Phys. Rev. B: Condens. Matter Mater. Phys.*, 2003, **68**, 085110.
11 P. Saint-Cast, D. Kania, M. Hofmann, J. Benick, J. Rentsch and R. Preu, *Appl. Phys. Lett.*, 2009, **95**, 151502.
12 J. Benick, B. Hoex, M. C. M. van de Sanden, W. M. M. Kessels, O. Schultz and S. W. Glunz, *Appl. Phys. Lett.*, 2008, **92**, 253504.
13 P. Saint-Cast, J. Benick, D. Kania, L. Weiss, M. Hofmann, J. Rentsch, R. Preu and S. W. Glunz, *IEEE Electron Device Lett.*, 2010, **31**, 695–697.
14 B. Liao, R. Stangl, T. Mueller, F. Lin, C. S. Bhatia and B. Hoex, *J. Appl. Phys.*, 2013, **113**, 024509.
15 J. Schmidt and A. Cuevas, *J. Appl. Phys.*, 1999, **85**, 3626–3633.
16 M. J. Kerr and A. Cuevas, *Semicond. Sci. Technol.*, 2002, **17**, 166–172.
17 S. de Wolf, G. Agostinelli, G. Beaucarne and P. Vitanov, *J. Appl. Phys.*, 2005, **97**, 063303.
18 M. Schaper, J. Schmidt, H. Plagwitz and R. Brendel, *Prog. Photovoltaics*, 2005, **13**, 381–386.
19 T. F. Schulze, H. N. Beushausen, C. Leendertz, A. Dobrich, B. Rech and L. Korte, *Appl. Phys. Lett.*, 2010, **96**, 252102.
20 S. de Wolf, B. Demaurex, A. Descoeudres and C. Ballif, *Phys. Rev. B: Condens. Matter Mater. Phys.*, 2011, **83**, 233301–233304.
21 A. Illiberi, M. Creatore, W. M. M. Kessels and M. C. M. van de Sanden, *Phys. Status Solidi RRL*, 2010, **4**, 206–208.
22 T. A. Li, S. Ruffell, M. Tucci, Y. Mansoulié, C. Samundsett, S. De Iullis, L. Serenelli and A. Cuevas, *Sol. Energy Mater. Sol. Cells*, 2011, **95**, 69–72.

 This journal is © the Owner Societies 2014

Published on 09 September 2014. Downloaded by National Physical Laboratory (NPL) on 24/04/2015 06:57:42.

23 K. O. Davis, K. Jiang, M. Wilson, C. Demberger, H. Zunft, H. Haverkamp, D. Habermann and W. V. Schoenfeld, *Phys. Status Solidi RRL*, 2013, **7**, 942–945.

24 T.-T. Li and A. Cuevas, *Phys. Status Solidi RRL*, 2009, **3**, 160–162.

25 C. Cibert, H. Hidalgo, C. Champeaux, P. Tristant, C. Tixier, J. Desmaison and A. Catherinot, *Thin Solid Films*, 2008, **516**, 1290–1296.

26 M. T. Seman, D. N. Richards, P. Rowlette and C. A. Wolden, *Chem. Vap. Deposition*, 2008, **14**, 296–302.

27 G. Dingemans and W. M. M. Kessels, *J. Vac. Sci. Technol., A*, 2012, **30**, 040802.

28 J. Wang, S. S. Mottaghian and M. F. Baroughi, *IEEE Trans. Electron Devices*, 2012, **59**, 342–348.

29 R. Lago-Aurrekoetxea, I. Tobías, C. del Cañizo and A. Luque, *J. Electrochem. Soc.*, 2001, **148**, G200–G206.

30 C. Berge, J. Schmidt, B. Lenkeit, H. Nagel and A. G. Aberle, 2nd World Conference on Photovoltaic Solar Energy Conversion, **1998**, 1426-1429.

31 N. Batra, Vandana, S. Kumar, M. Sharma, S. K. Srivastava, P. Sharma and P. K. Singh, *Sol. Energy Mater. Sol. Cells*, 2012, **100**, 43–47.

32 J. Lekner, *Theory of Reflection of Electromagnetic and Particle Waves*, Developments in Electromagnetic Theory and Applications, Springer Science Media Busniss BV, 1987, vol. 3 (ISBN 978-94-015-7748-9).

33 A. Nussbaum and R. A. Phillips, *Contemporary Optics for Scientists and Engineers*, Prince-Hall, Englewood Cliffs, NJ, 1974.

34 J. Zhao and M. A. Green, *IEEE Trans. Electron Devices*, 1991, **38**, 1925.

35 Vandana, N. Batra, P. Kumar, P. Sharma and P. K. Singh, *Mater. Chem. Phys.*, 2014, **144**, 242.

36 L. Favaro, A. Boumaza, P. Roy, J. Lédion, G. Sattonnay, J. B. Brubach, A. M. Huntz and R. Tétot, *J. Solid State Chem.*, 2010, **183**, 901–908.

37 R. Katamreddy, R. Inman, G. Jursich, A. Soulet and C. Takoudis, *J. Electrochem. Soc.*, 2006, **153**(10), C701–C706.

38 M. Ben Rabha, M. Salem, M. A. Khakani, B. Bessais and M. Gaidi, *Mater. Sci. Eng., B*, 2013, **178**, 695–697, DOI: 10.1016/j.mseb.2012.11.021.

39 Z. Katz-Tsameret and A. Raveh, *J. Vac. Sci. Technol., A*, 1995, **13**, 1121–1127.

40 A. W. Stephens and M. A. Green, *Sol. Energy Mater. Sol. Cells*, 1997, **45**, 255–265.

41 S. Kumar, P. K. Singh and S. R. Dhariwal, *Appl. Phys. Lett.*, 2010, **96**, 162109–162111.

42 B. Shin, J. R. Weber, R. D. Long, P. K. Hurley, C. G. Van de Walle and P. C. McIntyre, *Appl. Phys. Lett.*, 2010, **96**, 152908.